# A constitutive model for thermoplastics intended for structural applications

Mario Polanco-Loria[1,3], Arild Holm Clausen[2,3], Torodd Berstad[1,3] and Odd Sture Hopperstad[2,3]

[1] SINTEF Materials and Chemistry, NO-7465 Trondheim, Norway
[2] Department of Structural Engineering, NTNU, NO-7491 Trondheim, Norway
[3] Structural Impact Laboratory (SIMLab), Centre for Research-based Innovation, NO-7491 Trondheim, Norway

**Summary:**

This paper presents a hyperelastic-viscoplastic constitutive model for thermoplastics [1]. It is partly based on a model proposed by Boyce et al. [2]. The model involves a hyperelastic-viscoplastic response due to intermolecular resistance, and an entropic hyperelastic response due to re-orientation of molecular chains. A Neo-Hookean material model is selected for describing large elastic deformations. Moreover, the Raghava plastic yield surface [3] is introduced to capture the pressure sensitivity behaviour, and a non-associative visco-plastic flow potential is assumed for volumetric plastic strain control. The strain-rate effects are formulated in a format well-suited for structural applications. Finally, the intramolecular stiffness is represented with Anand's stress-stretch relation [4]. The model is developed within a framework developed for finite elastic and plastic strains, using a multiplicative decomposition of the deformation gradient. It is implemented as a user-defined model in LS-DYNA [5].
The material model requires 10 parameters which are easy to identify from true stress-strain curves obtained from uniaxial tension and compression tests. In this paper, the parameters are determined from experimental tests on a polyethylene material with high density (PEHD). Subsequently, the model is employed in numerical simulations of the uniaxial tension test and a quasi-static test on a centrally loaded plate. The numerical model gives satisfactory predictions when compared to the observed experimental behaviour.

**Keywords:**

Constitutive model, thermoplastics, hyperelastic, viscoplastic, experimental validation.

# 1 Introduction

Among the different classes of materials, i.e. metals, concrete, wood, polymers etc., few materials face the same world-wide increase in demand and use as polymers do. The current growth is closely related to several attractive properties of polymers: they are cheap, easy to form, have low density, they may be very ductile, and also, depending on additives and environment, be rather durable. In particular, polymers may have excellent energy absorption characteristics. Therefore, polymers are promising for use in many applications where other materials, e.g. metals, have been the common choice so far.

There are three main groups of polymers: Thermoplastics, thermosets and elastomers. All of them consist of long molecule chains with carbon atoms in the „backbone“. The bonding structure is, however, slightly different for the three groups. There are only weak van der Waals bonds between neighbour chains in thermoplastics, giving such materials a rather flexible structure facilitating large plastic deformations caused by relative sliding between the chains. On the other hand, inter-molecular covalent bonds, or cross-links, are present for thermosets and elastomers. While the latter group has approximately 1 cross-link connection per 1000 atoms of the main molecule chain, there is a considerably higher cross-link density in thermosets, may be 1 for every 20 atom in the backbone chain [6]. Therefore, thermosets are much stiffer than elastomers. Also, the cross-links imply a „memory effect“, ensuring that thermosets and elastomers behave elastic under most circumstances.

Thus, the difference in molecular structure has consequences for the behaviour of the polymer at hand, and also for the availability of material models for use in commercial finite element codes. While there exists rather accurate models for thermosets and elastomers, Du Bois et al. [7] claimed that the present models for thermoplastics still needed further improvements. Generally speaking, a material model for thermoplastics should be capable of handling large temperature and strain-rate effects, deformation-induced anisotropy, viscosity, and also other commonly observed features. Certainly, it is challenging to develop a material model which covers most of these phenomena, yet is sufficiently user friendly for industrial applications.

This paper presents a recently developed constitutive model for thermoplastics [1]. It involves 10 coefficients, and it is based on a model proposed by Boyce et al. [2], but with some modifications. Firstly, the energy-elastic deformation is represented with a Neo-Hookean model. Further, Raghava's pressure-dependent yield function is introduced [3], and a non-associated flow rule is assumed, applying a Raghava-like plastic potential. The entropy-elastic deformation is modelled with Anand's stress-stretch relation [4].

Some laboratory observations, including material tests and well-defined component tests, are also included in this paper because physical experiments are a necessary pre-requisite for development of new material models. Material tests are useful for two purposes. Firstly, they provide relevant information whose physical features a model should be able to represent. Moreover, material tests are required for calibration of the coefficients in a model. Thereafter, it is quite common to validate a proposed material model by doing numerical simulations of the component or at a structural level.

The next section of this paper provides a brief outline of the constitutive model. Next, material tests on a high-density polyethylene (PEHD) are reviewed, see Moura et al. [8] for further details. The results from these tests are used to calibrate the constitutive model. Finally, the model is employed in numerical simulations of a tension test and a centrally loaded plate under quasi-static conditions. The predictions are compared with experimental results.



# 2 Constitutive model

## 2.1 Overview

Figure 1 summarises the main constituents of the constitutive model [1]. The material response is assumed to have two Parts A and B, which represent the intermolecular and intramolecular strength, respectively. Parts A and B are kinematically described by the same deformation gradient. The Cauchy stress tensor is obtained by summing the contributions of Parts A and B, i.e. $\boldsymbol{\sigma} = \boldsymbol{\sigma}_A + \boldsymbol{\sigma}_B$. The model requires 10 parameters which are easy to identify from true stress-strain curves obtained in uniaxial tension and compression tests [1].

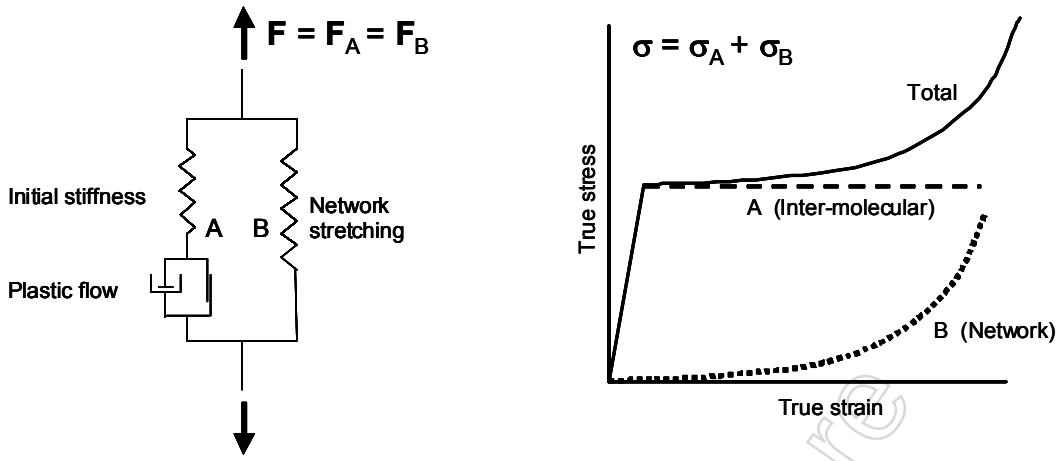


*Figure 1: Proposed constitutive model with inter-molecular (A) and network (B) contributions.*

### 2.2 Part A: Intermolecular resistance

The deformation gradient $\mathbf{F}_A$ is decomposed into elastic and plastic parts, i.e. $\mathbf{F}_A = \mathbf{F}_A^e \cdot \mathbf{F}_A^p$. Similarly, the Jacobian $J_A$ of Part A, representing the volume change, is decomposed as $J_A = \det \mathbf{F}_A = J_A^e J_A^p = J$. A compressible Neo-Hookean material is chosen for the elastic part of the deformation, and the Cauchy stress tensor $\boldsymbol{\sigma}_A$ reads

$$\boldsymbol{\sigma}_A = \frac{1}{J}\left(\lambda_0 \ln J_A^e \, \mathbf{I} + \mu_0[\mathbf{B}_A^e - \mathbf{I}]\right)$$

where $\lambda_0$ and $\mu_0$ are the classical Lamé constants of the linearized theory, $\mathbf{B}_A^e = \mathbf{F}_A^e \cdot (\mathbf{F}_A^e)^T$ is the elastic left Cauchy-Green deformation tensor, and $\mathbf{I}$ is the second order unit tensor. The coefficients $\lambda_0$ and $\mu_0$ may alternatively be expressed as functions of Young's modulus $E_0$ and Poisson's ratio $\nu_0$. The yield criterion is assumed in the form $f_A = \bar{\sigma}_A - \sigma_T = 0$, where $\sigma_T$ is the yield stress in uniaxial tension. The equivalent stress $\bar{\sigma}_A$ accounts for the pressure-sensitive behaviour, commonly observed in polymeric materials, and it is defined according to Raghava et al. [3], viz.

$$\bar{\sigma}_A = \frac{(\alpha-1)I_{1A} + \sqrt{(\alpha-1)^2 I_{1A}^2 + 12\alpha J_{2A}}}{2\alpha}$$

The material parameter $\alpha = \sigma_C / \sigma_T \geq 1$ describes the pressure sensitivity, where $\sigma_C$ is the uniaxial compressive yield strength of the material, and $I_{1A}$ and $J_{2A}$ are stress invariants related to respectively the total and the deviatoric Cauchy stress tensor. It is noted that the equivalent stress $\bar{\sigma}_A$ is equal to the von Mises – equivalent stress $\bar{\sigma} = \sqrt{3J_2}$ when $\alpha = 1$, i.e. $\sigma_C = \sigma_T$.

It turned out that an associated flow rule predicts unrealistic large volumetric plastic strains. In order to control the plastic dilatation, a non-associative flow rule is introduced. The Raghava-like plastic potential $g_A$ reads

$$g_A = \frac{(\beta-1)I_{1A} + \sqrt{(\beta-1)^2 I_{1A}^2 + 12\beta J_{2A}}}{2\beta} \geq 0$$

where the material parameter $\beta \geq 1$ controls the volumetric plastic strain. Isochoric plastic behaviour is obtained in the special case of $\beta = 1$.

Finally, the flow rule gives the plastic rate-of-deformation tensor as $\mathbf{D}_A^p = \dot{\bar{\varepsilon}}_A^p \, \partial g_A / \partial \boldsymbol{\sigma}_A$, where the equivalent plastic strain rate is chosen as

$$\dot{\bar{\varepsilon}}_A^p = \begin{cases} 0 & \text{if } f_A \le 0 \\ \dot{\varepsilon}_{0A} \left\{ \exp\left[ \frac{1}{C} \left( \frac{\bar{\sigma}_A}{\sigma_T} - 1 \right) \right] - 1 \right\} & \text{if } f_A > 0 \end{cases}$$

The two coefficients $C$ and $\dot{\varepsilon}_{0A}$ are easy to identify from uniaxial strain-rate tests.

### 2.3 Part B: Intramolecular resistance

The deformation gradient $\mathbf{F}_B$, see Figure 1, represents the network orientation and it is assumed that the network resistance is hyperelastic. Following Anand [4], the Cauchy stress-stretch relation is given as

$$\boldsymbol{\sigma}_B = \frac{1}{J} \left[ \frac{C_R}{3} \frac{\bar{\lambda}_L}{\bar{\lambda}} \mathcal{L}^{-1} \left( \frac{\bar{\lambda}}{\bar{\lambda}_L} \right) (\mathbf{B}_B^* - \bar{\lambda}^2 \mathbf{I}) + \kappa (\ln J) \mathbf{I} \right]$$

where the Jacobian $J = J_B = \det \mathbf{F}$, and $\mathcal{L}^{-1}$ is the inverse function of the Langevin function defined as $\mathcal{L}(\beta) = \coth \beta - 1/\beta$. The effective distortional stretch is $\bar{\lambda} = \sqrt{\mathrm{tr}(\mathbf{B}_B^*)/3}$, where $\mathbf{B}_B^* = \mathbf{F}_B^* \cdot (\mathbf{F}_B^*)^{\mathrm{T}}$ is the distortional left Cauchy-Green deformation tensor, and $\mathbf{F}_B^* = J_B^{-1/3} \mathbf{F}_B$ denotes the distortional part of $\mathbf{F}_B$. There are three constitutive parameters describing the intra-molecular resistance: $C_R$ is the initial elastic modulus of Part B; $\bar{\lambda}_L$ is the locking stretch; and $\kappa$ is a bulk modulus.

### 2.4 Numerical verification of the constitutive model

The proposed model is implemented as a user-defined model in LS-DYNA [5], so far working for solid elements. A set of numerical tests has been carried out [1], showing that the model is able to capture pressure dependency, volumetric plastic strain, strain rate sensitivity, and induced strain anisotropy.

## 3 Material tests and calibration

### 3.1 Material tests

Uniaxial material tests in tension and compression were carried out on a PEHD material delivered as 10 mm thick plates by the German company Simona. The tests were performed at respectively two and three different, yet quasi-static, rates [8].

A major challenge associated with material testing of ductile polymers is that they experience cold drawing in tension, meaning that a neck evolves along the whole gauge length of the sample before it eventually ruptures at a very large deformation. This means that an extensometer is not an adequate measurement tool. Also, different to metals, many polymers are susceptible to volume changes during plastic deformation. The practical consequence is that measurements of transverse strains are required in order to determine true stress. Therefore, we employed the Digital Image Correlation (DIC) technique in all tension and compression tests to facilitate in-plane full-field measurements and a subsequent deduction of true stress-strain curves.

Figure 2 shows test results obtained in the extrusion direction of the plate material. Two replicate tests were carried out when determining the true stress-strain curve at strain rate $10^{-3}$ $s^{-1}$, see Figure 2a. The transverse strain was measured in respectively the thickness and width direction of the plate in these two parallel tests, revealing that the transverse deformation is isotropic [8]. Also, it was found that the ratio between transverse and longitudinal strains was not significant different from 0.5 before the longitudinal strain exceeded 1, meaning that the plastic deformation of this PEHD material could be considered as isochoric.

Another set of samples was used in the strain-rate tests [1]. Although not shown in Figure 2, tests were also performed in other loading directions than the extrusion direction, but these showed that the material essentially can be considered as isotropic [8].

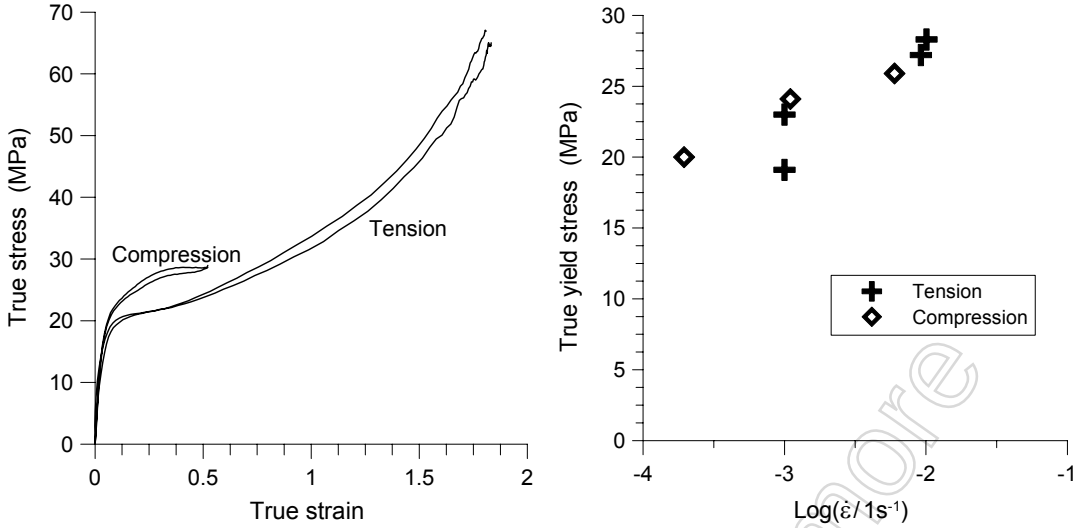


*Figure 2: Material tests on PEHD. (a) True stress-strain curves from tension and compression samples tested in the extrusion direction, strain rate $10^{-3}$ $s^{-1}$. (b) Strain-rate sensitivity of yield stress.*

### 3.2 Calibration of constitutive model

The test results were used to determine the parameters in the constitutive model, and their values are given in Table 1. As already noticed, the plastic dilatation of the material was close to zero, therefore, $\beta = 1$ and effectively a Mises-based flow rule was adopted. Because Figure 2b covers only two quasi-static decades of strain-rate, the value of the strain-rate coefficient $C$ must be viewed with some care. The present database of material tests is insufficient for simulations of high strain rate dominated problems (e.g. crash, impact). For such situations tension tests at elevated rates of strain should be carried out. Finally, the bulk modulus $\kappa$ was deliberately kept to zero in the calibration procedure, implying a deviatoric stress state in Part B of the model.

*Table 1. Calibrated material parameters for the PEHD material.*

| $E_0$ (MPa) | $\nu_0$ | $\sigma_T$ (MPa) | $\alpha$ | $\beta$ | $\dot{\varepsilon}_{0A}$ ($s^{-1}$) | $C$ | $C_R$ (MPa) | $\bar{\lambda}_L$ | $\kappa$ (MPa) |
|---|---|---|---|---|---|---|---|---|---|
| 700 | 0.48 | 19 | 1.267 | 1.0 | 0.001 | 0.15 | 2.0 | 31.62 | 0 |

## 4 Numerical examples

### 4.1 Tension test

Numerical simulations of the experimental tensile specimens, used for material model calibration, are reported in Figure 3. The deviations between the load-displacement curves obtained from the numerical and experimental tests are less than the experimental scatter reported in [8]. In addition, the necking extension after a displacement of 30 mm (see point A in Figure 3) is predicted relatively well by the numerical model, see Figure 4.

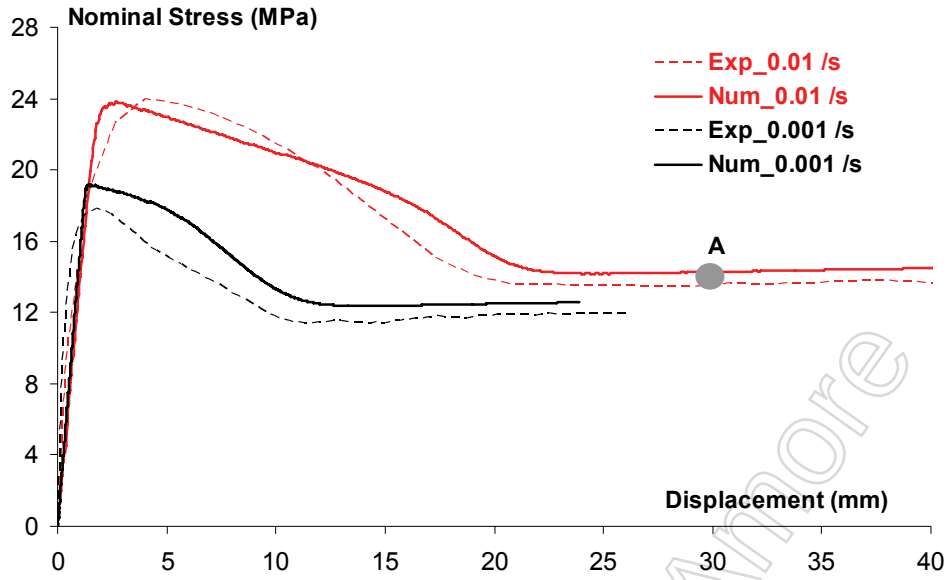


*Figure 3: Identification of material parameters and its comparison with experimental data.*

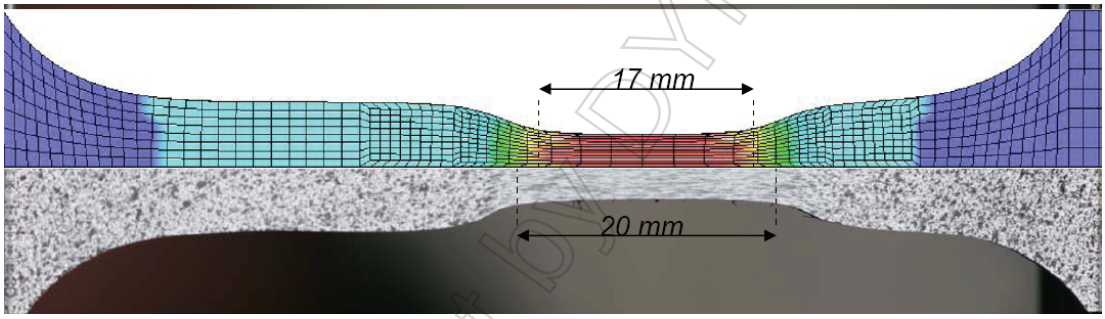


*Figure 4: Extension of neck after a displacement of 30 mm – numerical prediction and experimental observation.*

### 4.2 Plate impact test

A quasi-static bending test was carried out on a square PEHD plate with in-plane dimension 600mm x 600mm and thickness 5mm. The plate was clamped with two stiff rings holding the plate with 24 M16 bolts along a circle with diameter 500mm [8]. Hence, the tested component was considered as effectively clamped circular plate in the subsequent numerical simulations. The plate was loaded by an impactor in the centre. A cylinder of diameter 60mm and with a rounded end radius of 5mm was used as impactor nose [8]. The impactor had a constant velocity of 1mm/s, ensuring a quasi-static test condition.

The plate was modeled with four-node axisymmetric elements in the LS-DYNA simulation, using the constitutive model outlined in Section 2 and the material parameters given in Table 1. A reduced integration scheme and hourglass control were applied. The finite element mesh of the circular plate consisted of 8 elements through its thickness and 155 elements along the radius, see Figure 5. Refinement of the mesh did not have any major influence on the results. The steel impactor was assumed as a rigid material. Moreover, a frictionless 2D_automatic_surface_to_surface contact option of LS-DYNA was adopted. Mass scaling was used to reduce computational time. It was checked that the kinetic energy was only a small fraction of the total energy.

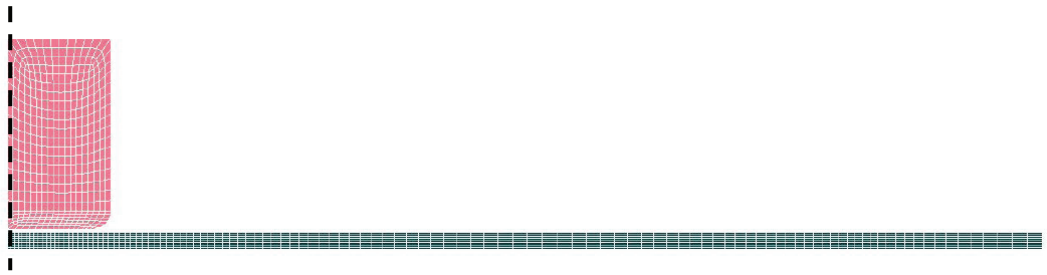

*Figure 5: 2D axisymmetric finite element model used in the numerical analysis.*

The force-displacement responses from the experimental test and numerical simulation are compared in Figure 6. The shape of the force-displacement curve is fairly well captured by the LS-DYNA model. The numerical analysis underestimates the load-carrying capacity of the plate by about 10 % in the quasi-static case. The non-linear stiffness observed in the test is well captured, where the initial elastic stiffness is gradually increased due to the membrane effect.

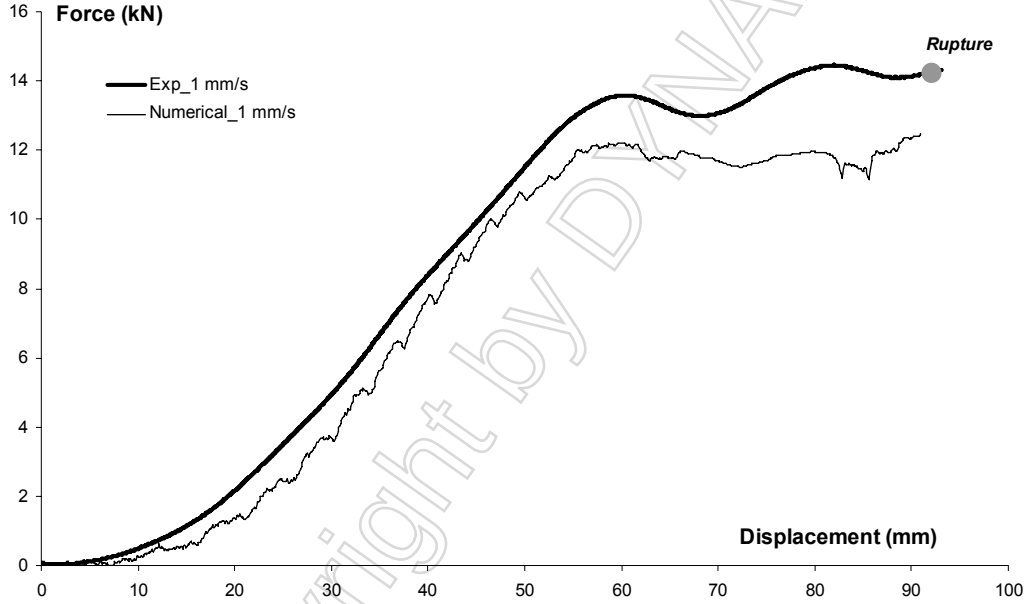


*Figure 6: Force-displacement curves obtained in experimental tests and numerical simulations.*

Failure was related to a deep-drawing mechanism forming a localized plug at the centre of the plate in the experimental test. This occurred at a displacement of about 93 mm, see Figure 7a. As illustrated in Figure 7b, this local behaviour is well captured by the numerical model, where the highly localized plastic strain distribution gives an idea of the cause of this failure mechanism.
The predictions presented herein must be considered as preliminary results obtained at a rather early stage of research. It is an obvious drawback that the maximum strain rate in the material tests was around $10^{-2}$ $s^{-1}$. Further, a more thorough modelling of the boundary conditions and initial plate imperfections (after mounting) may improve the results. It is also believed that the observed deviations could have been further clarified with introduction of friction effects between the impactor nose and the plate in the simulations. Some features of the constitutive model may also call for a closer investigation [1]. One potential amendment is to choose another formulation of the non-associated flow rule in the sliding element of Figure 1, yet this is probably a minor source of error in the simulations presented herein because the material turned out to behave almost isochoric during plastic deformation.

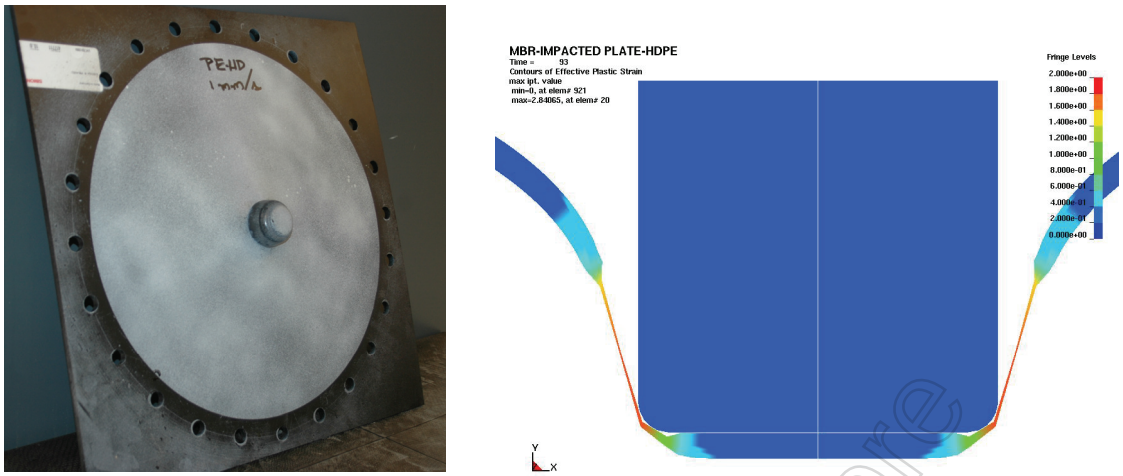


(a) (b)

*Figure 7: (a) Deformed plate with localized plug after quasi-static testing. (b) Localization around impactor in numerical simulation of a quasi-static test.*

## 5 Concluding remarks

This paper outlined a new hyperelastic-viscoplastic constitutive model for thermoplastics. The model consists of two fractions sharing the same deformation gradient, and accounting in turn for the intermolecular resistance by pressure-dependent, non-associated hyperelastic-viscoplasticity, and the network resistance by hyperelasticity for compressible rubber-like materials. All 10 parameters of the proposed model can be determined from uniaxial tension and compression tests at different strain rates, provided the true stress and true strains (axial and lateral) are continuously measured during the deformation process. Yet, some use of inverse modelling might be favourable in order to obtain an optimal fit to experimental observations. The constitutive relation is implemented as a user-defined model in LS-DYNA, currently working for brick elements.
After calibrating the constitutive model for a PEHD material, it was employed in numerical simulations of a tension test and a centrally loaded plate under quasi-static test conditions. The force-displacement curve as found in the experimental test was rather well captured in the simulations. Although there are uncertainties associated with the material model as well as the numerical modelling of the problem at hand, the results from this rather limited study are promising.

## 6 Literature

[1] Polanco-Loria M., Clausen A.H., Berstad T. and Hopperstad O.S.: "Constitutive model for thermoplastics with structural applications". Submitted for possible journal publication, 2009.
[2] Boyce M.C., Socrate C. and Llana P.G.: "Polymer", 41, 2000, 2183-2201.
[3] Raghava R., Caddell R.M. and Yeh G.S.Y.: "Journal of Materials Science", 8, 1973, 225-232.
[4] Anand L.: „Computational Mechanics“, 18, 1996, 339-355.
[5] Livermore Software Technology Corporation: "LS-DYNA Keyword User's Manual. Version 971.", 2007.
[6] Ehrenstein G.W.: "Polymeric Materials. Structure – Properties – Applications", Carl Hanser Verlag, 2001.
[7] Du Bois P.A., Kolling S., Koesters M., Frank T.: "International Journal of Impact Engineering", 32, 2006, 725-740.
[8] Moura R.T., Clausen A.H., Fagerholt E., Alves M. and Langseth M.: "Impact on PEHD and PVC plates – Experimental tests and numerical simulations". Submitted for possible journal publication, 2009.